JCTC Journal of Chemical Theory and Computation

Article

pubs.acs.org/JCTC

Highlights on Anthocyanin Pigmentation and Copigmentation: A Matter of Flavonoid π-Stacking Complexation To Be Described by DFT-D

Florent Di Meo,[†] Juan Carlos Sancho Garcia,[‡] Olivier Dangles,[§] and Patrick Trouillas*[,†,∥]

[†]Université de Limoges, LCSN-EA 1069, Faculté de Pharmacie, 2 rue du Docteur Marcland, F-87025 Limoges, France

[‡]Departamento Química Física, Universidad de Alicante, Ap. De Correos 99, E-03080, Alicante, Spain

[§]University of Avignon, INRA, UMR408, 84000, Avignon, France

[∥]Laboratoire de Chimie des Matériaux Nouveaux, Université de Mons, Place du Parc 20, B-7000 Mons, Belgium

Supporting Information

ABSTRACT: Anthocyanidins are a class of π-conjugated systems responsible for red, blue, and purple colors of plants. They exhibit the capacity of aggregation in the presence of other natural compounds including flavonols. Such complexations induce color modulation in plants, which is known as copigmentation. It is largely driven by π-interactions existing between pigments and copigments. In this work, the energies of copigmentation−complexation and self-association are systematically evaluated for an anthocyanidin/flavonol couple prototype (3-*O*-methylcyanidin/quercetin). To describe noncovalent interactions, DFT-D appears mandatory to reach a large accuracy. Due to the chemical complexity of this phenomenon, we also aim at assessing the relevance of both B3P86-D2 and ωB97X-D functionals. The benchmarking has shown that B3P86-D2 possesses enough accuracy when dealing with π−π interactions with respect to both spin component scaled Møller−Plesset second-order perturbation theory post Hartree−Fock method and experimental data. UV−vis absorption properties are then evaluated with time-dependent DFT for the different complexes. The use of range-separated hybrid functionals, such as ωB97X-D, helped to correctly disentangle and interpret the origin of the UV−vis experimental shifts attributed to the subtle copigmentation phenomenon.

1. INTRODUCTION

More than 8000 different natural polyphenols (e.g., flavonoids, lignans, depsides, coumarins, oligomers, and polymers) have been isolated from the plant kingdom; all plant organs being concerned (e.g., leaves, fruit, roots, and flowers). Therefore they are relatively abundant in human diets (e.g., fruit, vegetables, spices, and beverages including tea, wine, and beer). Apart from their important biological activities in plants and potential health benefits in humans (e.g., prevention of cardiovascular,[1] neurodegenerative[2] and hepatic diseases,[3,4] and possibly some cancers),[5] some polyphenols are responsible for fruit/beverage/flower/leaf coloration.[6,7] The UV−vis absorption characteristics of polyphenols taking part in plant colors are well established from both experimental and theoretical points of view.[8,9]

Anthocyanins belong to the flavonoid subclass and are responsible for red, blue, and purple colors of many flowers (e.g., orchids, tulips, roses, and many blue flowers), leaves (e.g., veins of tobacco leaves), fruit (e.g., grapes, berries, and tomatoes), and vegetables (e.g., tomatoes and aubergines). Around one thousand of such pigments have been evidenced so far. Anthocyanins are glycosides of so-called anthocyanidins, which are flavylium (2-phenyl-1-benzopyrylium) ions substituted by several OH and OMe groups.[10,11] Additionally, the sugar moieties are frequently acylated by a variety of aliphatic and aromatic carboxylic acids including acetic, *p*-coumaric, and caffeic acids (as in *Vitis vinifera* L. grape). The red color of anthocyanins is mainly attributed to the flavylium cation (AH^+), which prevails at pH < 4. At pH 4−6, the most acidic groups of AH^+ (positions 4′, 5, and 7) are deprotonated, thus giving a mixture of neutral tautomeric quinoid bases A (purple). At pH > 6, a second deprotonation can take place forming anionic quinoid bases A^- (blue). Besides fast proton-transfer equilibria, AH^+ also undergoes water addition at position 2 with formation of a colorless hemiketal (B), itself in equilibrium with minor amounts of pale yellow (*Z*)- and (*E*)-chalcones (C).[12] Although water addition is much slower than proton transfer, the colorless hemiketal is typically the thermodynamic, most stable form in mildly acidic solutions (pH > 2−3), in the case of common anthocyanins. Thus, the persistence of bright colors in plants under such conditions (nonextreme low pH) clearly suggests that natural mechanisms of color stabilization operate. The flat polarizable chromophores of the colored forms (mainly AH^+) are quite prone to π-stacking interactions with themselves (self-association) and with the pool of colorless polyphenols (especially, flavones, flavonols, and hydroxycinnamic acids) coexisting with anthocyanins in the vacuoles of plant cells.[13−17] The latter binding phenomenon is so-called copigmentation, being evidenced, e.g., by the diamagnetic shifts of NMR signals pertaining to the aromatic protons of the pigment and copigment molecules when they associate.[18] Being maximized in aqueous solution (weakened by organic cosolvents) and weakly affected by the ionic strength, copigmentation must be mainly driven by van der Waals interactions and hydrophobic effects, although H-bonding

Received: January 30, 2012
Published: May 1, 2012

Scheme 1. Chemical Structures of (a) 3-*O*-Methylcyanidin and (b) Quercetin

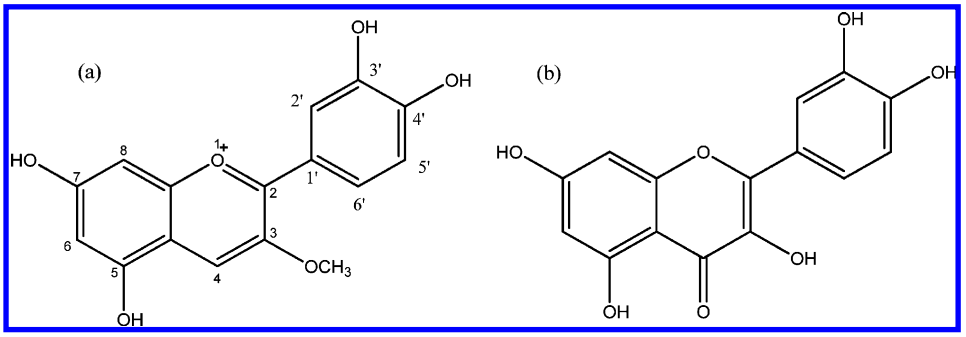

between the pigment and copigment molecules may contribute.[19,20]

π-Stacking was suggested as the major contribution to molecular complexation of aromatic ligands. An offset geometry for the two partners within the complex is usually favored so as to minimize unfavorable repulsions of π-electrons.[21] π-Stacking may be important (i) in organic chemistry contributing to regio- and stereoselectivity,[22,23] (ii) in material science explaining charge-transfer (CT) phenomena,[24,25] and supramolecular organization issues[21] or iii) in biology contributing to ligand−protein and ligand−nucleic acid interactions.[26] Although the major role of π-stacking interactions in copigmentation has sound experimental support,[27−31] it is still unclear how they take part in color variation. Indeed, copigmentation not only displaces the hydration equilibrium toward the flavylium ion, thereby resulting in a hyperchromic shift, but is also known to shift the visible absorption band of anthocyanins to higher wavelengths. The role of π-stacking interactions in this typical bathochromic(red)-shift is still not completely understood.

The present work aims at describing and rationalizing π-stacking interactions and the subsequent light absorption properties using state-of-the-art computational methods, i.e., time-dependent density functional theory (TD-DFT), with functionals accurately describing dispersive effects and CT. For this purpose we used a prototypical couple of flavonoid pigment/copigment that may form π-stacking complexes: 3-*O*-methylcyanidin and quercetin, a very common flavonol (Scheme 1), were chosen as the anthocyanin pigment and copigment, respectively; the methyl group being chosen to model the electronic effect of the sugar moiety at a lower computational cost. Both compounds can be considered as the two interacting moieties of many pigment and copigment couples found in nature.[13,30,32] When both quercetin and cyanidin derivatives are present in aqueous solution, they can in principle bind (copigmentation) or self-associate (formation of noncovalent dimers). A large set of relevant properties, such as interaction energies, CT, and UV−vis properties, were investigated for the copigmentation complex [3-*O*-methylcyanidin:quercetin] (**C:Q**) and both dimers [3-*O*-methylcyanidin]$_2$ (**C:C**) and [quercetin]$_2$ (**Q:Q**). Copigmentation has thus been rationalized by comparing the UV−vis properties of the complexes with those of the free flavonoids.

To achieve these goals, the manuscript is structured as follows: Section 2 carefully describes the computational methodology employed. Section 3 shows further computational details concerning the choice of the theoretical method after a detailed benchmark study. Section 4.1 first describes geometries and energies of all stable complexes. A detailed analysis of the different binding contributions (i.e., dispersive, H-bonding, and electrostatic) is next proposed. The CT excited state and UV−vis properties are then discussed in Section 4.2 to rationalize copigmentation by flavonols. Note that throughout text, as well as within the concluding section, the robustness of the cost-effective theoretical methodology used is discussed with respect to both high-level calculations and experimental observations.

2. METHODOLOGY

Over the past years, quantum chemistry calculations have emerged as a relevant tool to provide accurate pictures of both π-stacking complexes[33] and optical properties.[25] DFT is particularly well adapted for medium-sized molecular systems and hybrid functionals permit accurate descriptions of many different chemical systems. For instance, B3P86 is particularly well adapted to calculate both thermodynamic[34,35] and UV−vis absorption properties[8] of isolated polyphenols. However, standard hybrid functionals are known to poorly reproduce (i) noncovalent weak interactions, such as π-stacking of conjugated systems, and (ii) (CT) in excited states. Both properties are of particular importance to understand copigmentation and must be therefore accurately described. Fortunately, new methods have been recently developed to correct these two generalized drawbacks of common functionals.[36,37]

Dispersion interaction arises from instantaneous fluctuations of locally induced dipole moments. To accurately model this system, the so-called van der Waals correlation functionals explicitly incorporate nonlocality (i.e., kernels depending simultaneously on r and r') effects in an accurate way.[38] Parameterized functionals have also been developed to calculate these nonbonded interactions, M06-2X being possibly among the most advanced fine-tuned expressions.[39] Another successful approach circumvents the use of these sophisticated correlation kernels by adding a dispersion correction based on the well-known dependence of the interactions between weakly overlapping systems as a function of the interatomic distance R:

$$E_{\mathrm{disp}} = -C_6/R^6 - C_8/R^8 - C_{10}/R^{10} \quad (1)$$

which is normally truncated after the first (or eventually the second) term and properly renormalized. The approach, originally developed by Grimme and called DFT-D,[37] can be efficiently coupled with any existing DFT-based method. It appears particularly relevant to calculate noncovalent interactions within an acceptable accuracy/computational time ratio.[40,41] Pairwise-like dispersion energy (E_{disp}) is thus calculated separately in a post self-consistent field fashion:

$$E = E_{\mathrm{DFT}} + E_{\mathrm{disp}} \quad (2)$$

where E_{disp} is a dispersion correction having the expected R_{AB}^{-6} dependent decay:

$$E_{disp} = -s_6 \sum_{A}^{N-1} \sum_{B>A}^{N} \frac{C_6^{AB}}{R_{AB}^6} f_{dmp}(R_{AB}) \quad (3)$$

where s_6 is a functional-dependent scaling factor, C_6^{AB} is the dispersion coefficient for the atomic pair AB, R_{AB} is the interatomic distance for atoms A and B, and $f_{dmp}(R_{AB})$ is a damping function that avoids near-singularities for small interatomic distances.[41] The refined version DFT-D2 has been widely used over the past years.[41] More recently the DFT-D3 version included atom pairwise-specific dispersion coefficients and a new set of cutoff radii as defined in the damping function.[42]

As quoted above, the uncorrected B3P86 method has been repeatedly applied before to the flavonoids tackled here with great success;[8,34,43] however, the copigmentation issue requires an accurate evaluation of the noncovalent interactions dominating the final shape of the dimers. To keep consistency with the previous studies, the specific parametrization of s_6 for the B3P86-D2 functional was achieved (see Section 3).

Once the ground-state structure of the complexes has been elucidated, its excited-state description can be done through the use of range-separated hybrid (RSH) functionals (e.g., CAM-B3LYP and ωB97).[44,45] This new family of functionals has been recently developed for an improved description of mainly Rydberg and CT excitations within the TD-DFT framework. The key point of RSH functionals is to split the $1/r_{ij}$ particle−particle operator entering into the Hamiltonian into controlled short- and long-range components, using the standard error function:

$$\frac{1}{r_{ij}} = \frac{1 - \mathrm{erf}(\omega r_{ij})}{r_{ij}} + \frac{\mathrm{erf}(\omega r_{ij})}{r_{ij}} \quad (4)$$

where r_{ij} is the interelectronic distance, and ω is a parameter defining the range separation. Different combinations of density-based and exact-like exchange functionals as a function of the interelectronic distance can be used. RSH functionals including ωB97 and ωB97X are known to definitely improve excited-state CT predictions.[24,46] Since the CT properties are known to be dramatically affected by the self-interaction error of standard hybrid functionals, this strategy is also known to partly tackle this problem. The ωB97 functional were also corrected to better describe noncovalent interactions, including empirical dispersion terms (ωB97X-D).[47]

Therefore geometry optimizations were performed using both B3P86-D2 and ωB97X-D functionals with the ORCA[48] and Gaussian09[49] packages, respectively. Excited states (ES) and the corresponding energies were obtained in the TD-DFT framework (with B3P86 and ωB97X-D). In order to assess the most adapted functional to describe copigmentation, in which CT may play an important role, results obtained with B3P86 were carefully compared to those obtained with the RSH functional ωB97X (see notes in text below).

The cc-pVDZ basis set has been used as it provides a good compromise between accuracy and computational time, regarding the size of the systems studied here. All DFT-D calculations (except those performed with ωB97X-D) have been achieved within the RIJCOSX approximation largely decreasing the computational time with a negligible error. This approach consists in using auxiliary basis sets to efficiently calculate exchange and coulomb matrices in the framework described by Neese et al.[50]

The intermolecular interaction energies were calculated as follow:

$$\Delta E_{int} = E_{complex} - \sum_{i}^{\text{free partner}} E_i \quad (5)$$

where $E_{complex}$ denotes the energy of the complex, and the summation runs over the two free partners. $E_{complex}$ included the basis set superposition error (BSSE), estimated using the traditional counterpoise method:

$$\mathrm{BSSE} = [E_{AB}^{AB}(A) - E_{A}^{AB}(A)] + [E_{AB}^{AB}(B) - E_{B}^{AB}(B)] \quad (6)$$

where E_{AB}^{AB} (A) and E_{AB}^{AB} (B) are the energies of two given free partners A and B, respectively, as obtained in the AB complex geometry with the AB basis set, and E_{A}^{AB} (A) and E_{B}^{AB} (B) are the energies of A and B, respectively, as obtained in the AB complex geometry with the A and B basis sets, respectively.

A comparison between Mulliken, ESPdipole[51,52] and CHelpG[53,54] population analysis is also done in Section 3, to avoid any possible CT overestimation provided by Mulliken densities.

Solvent effects were taken into account using implicit solvent models, in which the solute is embedded in a shape-adapted cavity surrounded by a dielectric continuum, which is characterized by a dielectric constant. Water (ε = 78.35) was used to reproduce the polar compartment (vacuoles) in which anthocyanins are concentrated in plant. Conformational analysis and interaction energies performed with the B3P86-D2 functional were performed using conductor-like screening nodel (COSMO)[55] model, while the polarizable continuum model[56,57] (PCM) was used with the other functionals. For TD-DFT calculations, the classical use of implicit solvent can be applied but may suffer from a fundamental problem, ignoring the time dependence of solvent relaxation (in particular the fast electron response, corresponding to the nonequilibrium solvent regime). An effective state-specific (SS) approach has been developed and has been shown to accurately describe the solvation free energy of a specific excited state.[58]

3. COMPUTATIONAL DETAILS

3.1. s_6 Grimme's Parameter Assessment. The dispersion correction of B3P86 mainly depends on s_6 as defined in eq 3. There is no assessed s_6 value available for B3P86-D2. An optimum value is found for the nonhybrid form, namely BP86 (s_6 = 1.05). However it may slightly deviate from the optimum value when a fraction of exact HF-like exchange is introduced (20% HF, in the case of B3P86). The s_6 optimization procedure is usually assessed on model systems including: (i) the potential energy curve for some rare-gas dimer dissociation and/or (ii) the S22 database[59,60] that includes noncovalent complexes. A set of s_6 values ranging from 1.05 to 0.65 was tested on S22 (see Supporting Information, Table S1). This range was motivated because s_6 decreases by 0.15 from BLYP to B3LYP (20% HF).[41] The standard mean average deviation (MAD) obtained with the entire S22 set was largely reduced, reaching chemical accuracy (MAD of 0.87 kcal·mol^{-1}) for the optimum 0.780 value (see Supporting Information, Table S1). The S22 database can be decomposed into three subgroups namely H-bond, true dispersion, and mixed electrostatic interactions.[60] The s_6 optimization procedure only slightly MAD decreased for the H-bond subgroup, while it was dramatically improved for

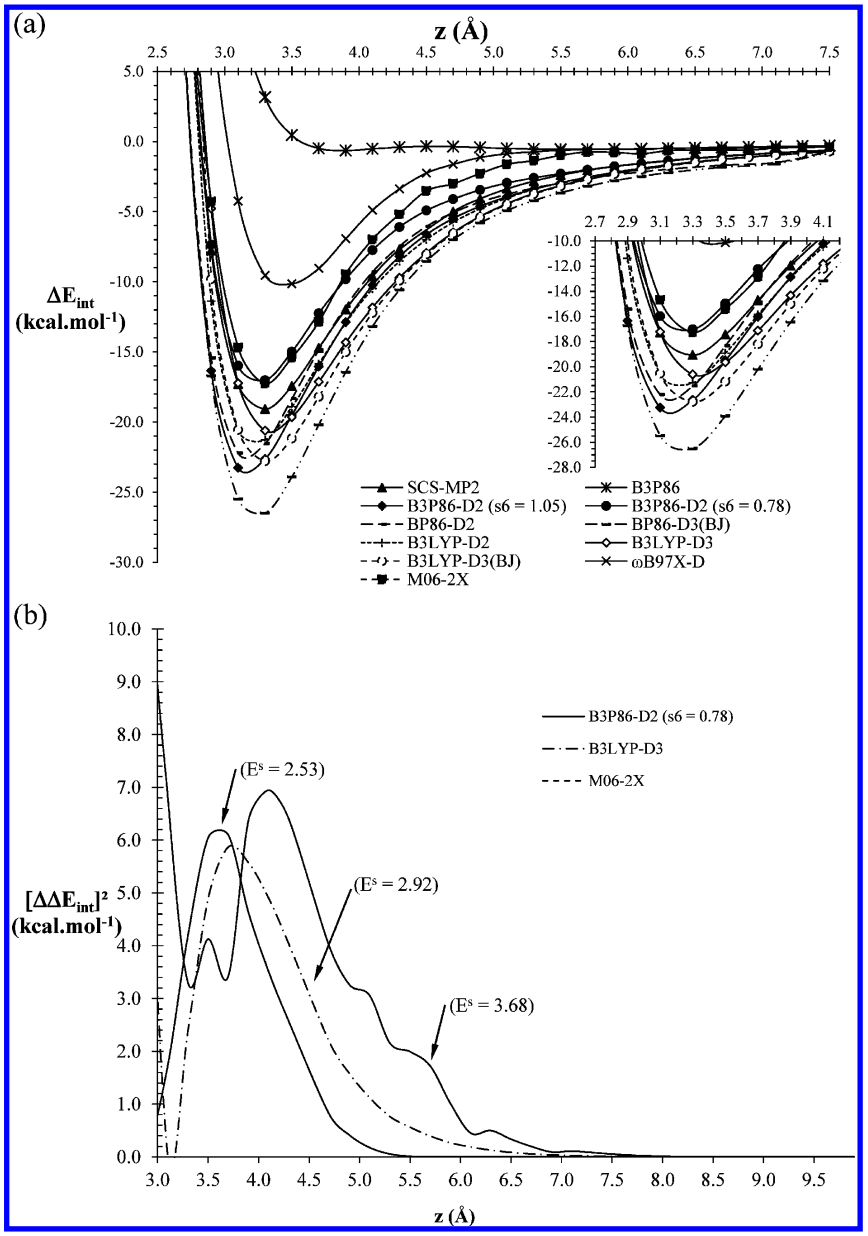

Figure 1. (a) Potential energy curves of the **C:Q** complex as obtained with different functionals. (b) Square differences ($[\Delta\Delta E_{int}]^2$) between the DFT and SCS-MP2 energies.

the other two subgroups. The basis set employed (cc-pVTZ) is believed to be close to the asymptotic region, additional calculations with the nearly exact def2-QZVP basis set provided a very similar MAD (0.76 kcal·mol^{-1}).

To validate the entire model, the potential energy curve of the **C:Q** complex was assessed with B3P86-D2 (default and optimized s_6 parameter) and compared to B3P86, BP86-D2, BP86-D3(BJ), ωB97X-D, B3LYP-D2, B3LYP-D3(BJ), B3LYP-D3, M06-2X, and spin component scaled Møller−Plesset second-order perturbation theory (SCS-MP2)[61,62] (Figure 1a). The cc-pVDZ basis set was chosen to reach enough accuracy at a reasonable computational cost, regarding the size of the system. The SCS-MP2/cc-pVDZ potential curve (taken here as an accurate reference) exhibited a minimum of −19.1 kcal·mol^{-1} at 3.3 Å (Figure 1a). As expected, the uncorrected B3P86 functional failed to qualitatively describe this potential energy curve (Figure 1a), exhibiting a dramatic underestimation of noncovalent interaction energies (ΔE_{int} of −0.6 kcal·mol^{-1}). The use of a too high s_6 parameter (i.e., s_6 = 1.05) stressed a minimum of −23.3 kcal·mol^{-1} at 3.1 Å (Figure 1a), which suggests the overestimation of noncovalent interaction energies and the corresponding underestimation of optimum intermolecular distances. The decrease of the s_6 parameter to the optimum value (0.780) significantly improved the $\pi-\pi$ complex stabilization exhibiting a minimum of −17.0 kcal·mol^{-1} at 3.3 Å (Figure 1a).[63] BP86-D2, BP86-D3(BJ) and B3LYP-D3(BJ) significantly overestimated the noncovalent interaction energies (ΔE_{int} of −22.2, −26.5, and −22.8 kcal·mol^{-1} at 3.1, 3.3, and 3.3 Å for the three functionals, respectively). The RSH functional ωB97X-D provided a too low interaction energy (−10.1 kcal·mol^{-1} at 3.4 Å, see Figure 1a). B3LYP-D3 and M06-2X provide a relatively accurate evaluation of the minimum (−20.6 and −17.3 kcal·mol^{-1} at 3.3 and 3.3 Å for both functionals, respectively, as seen in Figure 1a).

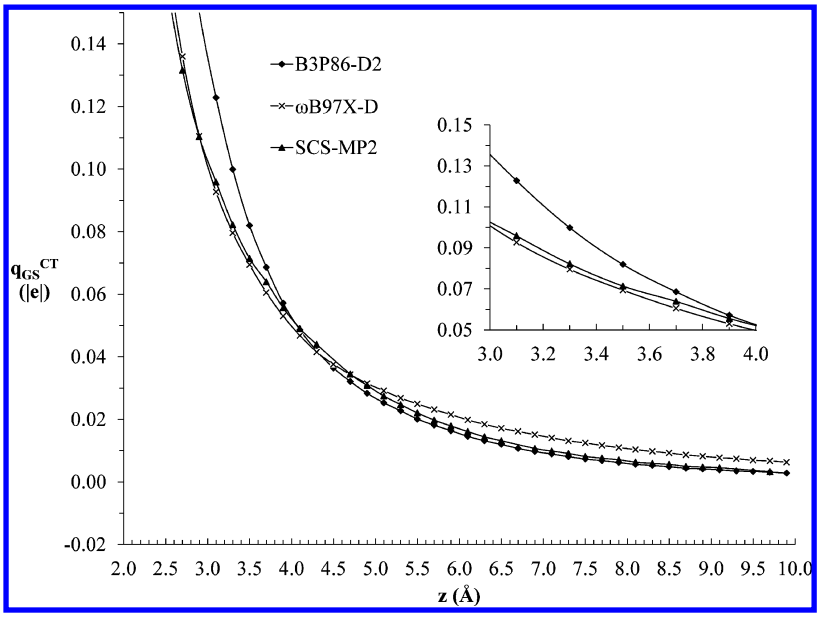

Figure 2. Ground-state CT for the antiparallel **C:Q** at the B3P86, B3P86-D2 (with default and optimum s_6 parameters), and ωB97X-D. The SCS-MP2 curve is shown as a reference. The cc-pVDZ was used for calculations shown here.

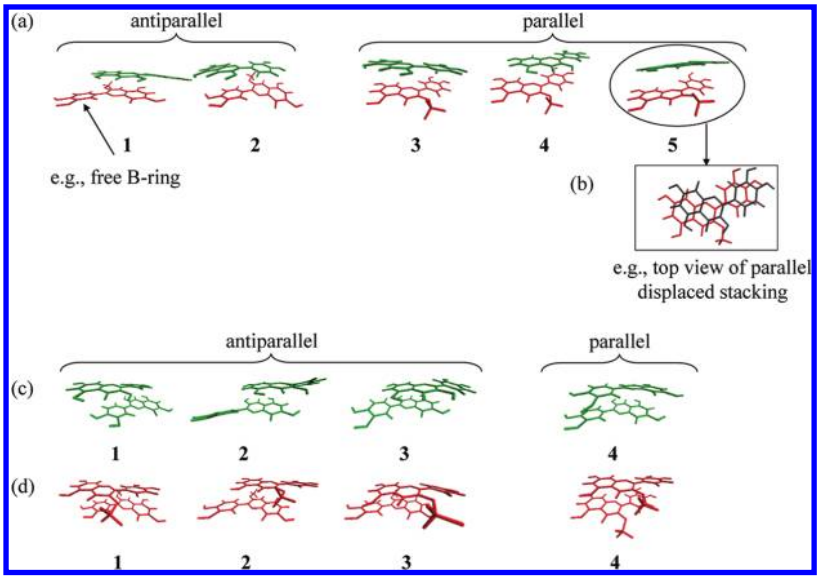

Figure 3. Optimized (COSMO-B3P86-D2(s_6 = 0.780)/cc-pVDZ) geometries for (a,b) **C:Q**, (c) **Q:Q**, and (d) **C:C**.

A thorough comparison of B3P86-D2(s_6 = 0.780), B3LYP-D3 and M06-2X were performed with respect to SCS-MP2 (Figure 1b). The most accurate methods appear to be B3P86-D2(s_6 = 0.780) and B3LYP-D3, as judged for instance by the surface error E^S,[64] which turns to be 2.5 and 2.9 kcal·mol^{-1} (Figure 1b). Note that the agreement between these two methods and the SCS-MP2 results is better around the equilibrium region (i.e., at 3.3 Å) although deteriorates for longer distances in favor of B3P86-D2(s_6 = 0.780). On the other hand, M06-2X provided a 'noisy' potential energy curve, which has already been described in certain cases and attributed to the high number parameters used to define this functional.[36]

3.2. CT Assessment. Ground-state CT between interacting partners is a main characteristic of $\pi-\pi$ molecular complexes. It is well admitted that for aromatic systems, charge analysis is better described by Class III methods, such as CHelpG.[65] Therefore this method was consequently used here to evaluate CT (q_{GS}^{CT}) with B3P86-D2, ωB97X-D, and SCS-MP2/cc/pVDZ. SCS-MP2/cc-pVDZ exhibited q_{GS}^{CT} of 0.09 |e| at the optimum intermolecular distance (i.e., z = 3.3 Å) (Figure 2), while both functionals provided very satisfactory results (0.12 and 0.08 |e| for B3P86-D2 and ωB97X-D, respectively).

All in all, these results showed that B3P86-D2 with an optimized s_6 parameter (0.780) might well serve as a reliable method to systematically explore potential energy surfaces of $\pi-\pi$ flavonoid complexation, whereas ωB97X-D is expected to accurately deal with CT excitations as we will show next.

4. RESULTS AND DISCUSSION

4.1. Geometry of $\pi-\pi$ Complexes. *Potential Energy Surface Exploration.* Due to the asymmetry of the 2-phenyl-1-benzopyrane nuclei of quercetin and 3-*O*-methycyanidin (see Scheme 1), two possible orientations were investigated, i.e., parallel and antiparallel (also called head-to-head or head-to-

tail, respectively). In the aim of exploring the entire potential energy surface for both orientations, the potential energy curve was first studied along the *z*-axis, i.e., following the distance separating both flavonoids. The minimum energy distance (z_{min}) appears higher for the parallel than for the antiparallel orientations (e.g., for **C:Q**, z_{min} = 3.5 and 3.3 Å for both orientations, respectively). The (*x*,*y*) potential energy surface was then explored at z_{min} (see Supporting Information, Figure S2). Five, four, and four orientations were obtained for **C:Q**, **Q:Q**, and **C:C**, respectively (Figure 3).

Optimized Geometries. For the antiparallel $\pi-\pi$ complexes, C-ring interacts either with B-ring (orientation **2** of **C:Q**, orientation **1** of **Q:Q**, and orientation **1** of **C:C**) or with A-ring (orientation **1** of **C:Q**, orientations **2**−**3** of **Q:Q**, and orientations **2**−**3** of **C:C**) (Figure 3). In the latter case (interaction between A- and C-rings), B-ring only interacts with the solvent (Figure 3). For the parallel $\pi-\pi$ complexes (orientations **3**−**5** of **C:Q**, orientation **4** of **Q:Q**, and orientation **4** of **C:C**), the whole tricyclic nuclei of both flavonoids interact with each other (Figure 3). As usually observed in $\pi-\pi$ complexes, no strict cofacial (face-to-face) arrangement occurs[66] but only the so-called parallel-displaced one (orientations **3**−**5** of **C:Q**, orientation **4** of **Q:Q**, and orientation **4** of **C:C**) (Figure 3).

Binding Energies. All the 13 orientations exhibit considerable binding energies (Table 1); **C:Q** being more stable than both dimers (by 1−3 kcal·mol^{-1}). **Q:Q** is more stabilized than **C:C** by around 1 kcal·mol^{-1} (Table 1). The five conformers of **C:Q** are very similar in energy, orientation **5** being slightly more probable according to the Boltzmann distribution (44.0%, see Table 1). These energies are in perfect agreement with the −13.9 kcal·mol^{-1} experimental binding enthalpy obtained for the **C:Q** complex.[67,20] This agreement confirms again the robustness of the BSSE-corrected B3P86-D2(s_6 = 0.780)/cc-pVDZ method to evaluate stability of polyphenol π-stacking complexes.

Taking all possible orientations into account for copigmentation complexes and both noncovalent dimers, the global Boltzmann distribution is 81, 1, and 18% for **C:Q**, **Q:Q**, and **C:C**, respectively. Anthocyanin self-association is also a mechanism that competes with water addition on the flavylium ion, thereby resulting in color stabilization. The relative contribution of anthocyanin copigmentation and self-association to color stability is of course dependent on the relative concentrations of pigment and copigment. With a potent copigment, such as quercetin, the higher stability of the **C:Q** copigmentation complex in comparison to the **C:C** anthocyanin dimer obtained in this work suggests that at equal pigment and copigment concentrations, copigmentation is the prevalent mechanism.

Contributions to Total Binding Energy. Our calculations suggest that H-bonding subtly participates in copigmentation. All intermolecular H-bonds observed in the copigmentation complex are relatively weak, with distances higher than 2.0 Å. Although weak, the H-bonds significantly change the planarity of 3-*O*-methylcyanidin (e.g., the dihedral angle between the C- and B-rings is −175.5° for free 3-*O*-methylcyanidin, while it is −159.0 and −161.3° for orientations **2** and **5** of **C:Q**, respectively). Nonetheless, H-bonding is not the most important contribution to the intermolecular interactions between quercetin and 3-*O*-methylcyanidin. Several orientations (orientations **1**, **3**, and **4** of **C:Q**, orientation **3** of **Q:Q**, and orientations **1** and **2** of **C:C**) do not present any H-bond, while their binding energies are in the same range as for the other orientations (see Table 1). The dispersive contribution is definitely the most important contribution to copigmentation complex formation with quercetin. The relative Grimme's dispersive energies are −25.6, −23.4, and −24.7 kcal·mol^{-1}, for **C:Q**, **Q:Q** and **C:C**, respectively, which is attributed to the large π-electron delocalization in each partner allowing strong London forces.

Finally, quantum calculations also shed light on the paradox of **C:C** dimers. As already described for other molecular systems,[68] there exist four optimal $\pi-\pi$ rearrangements in which dispersion compensates the strong Coulomb repulsion: taking the first-order terms, the average Coulomb and dispersion energies are +27.2 and −24.7 kcal·mol^{-1}, respectively.

Ground-State CT. At equilibrium distance, ground-state CT is observed from quercetin to 3-*O*-methylcyanidin (q_{GS}^{CT} around 0.06 |e|, see Table 2a). As a powerful free radical

Table 1. Counterpoise-Corrected Binding Energies (ΔE_{int}, kcal·mol^{-1}) and Boltzmann Weights (D_{bolt}) Calculated for the Most Stable Geometries of C:Q, Q:Q, and C:C with COSMO-B3P86-D2(s_6 = 0.780)/cc-pVDZ

complex	orientation	ΔE_{int}	D_{bolt} (%)
C:Q	1	−13.3	16.2
	2	−13.1	12.9
	3	−12.8	7.0
	4	−13.4	19.9
	5	−13.9	44.0
Q:Q	1	−11.1	27.1
	2	−9.1	0.9
	3	−10.6	11.6
	4	−11.6	60.4
C:C	1	−12.7	30.5
	2	−12.9	41.7
	3	−11.9	7.7
	4	−12.5	20.2

Table 2. CT Ground (q_{GS}^{CT}, |e|) and Excited (q_{ES}^{CT}, |e|) States, Total CT (q^{CT}, |e|), Dipole Moment of Ground (μ_{GS}, D) and Excited (μ_{ES}, D) States, and Absolute Dipole Variation ($|\Delta\mu|$, D) of Optimized C:Q, Q:Q, and C:C Complexes[a]

complex	orientation	q_{GS}^{CT}	q_{ES}^{CT}	q^{CT}	μ_{GS}	μ_{ES}	$\lvert\Delta\mu\rvert$
C:Q	1	0.07	0.02	0.09	8.3	7.8	0.5
	2	0.06	0.00	0.06	16.2	16.6	0.4
	3	0.05	0.08	0.13	9.1	7.8	1.3
	4	0.05	0.25	0.30	9.9	4.8	5.1
	5	0.05	0.68	0.73	9.0	6.5	2.4
Q:Q	1	0.00	0.00	0.00	0.0	0.0	0.0
	2	0.00	0.00	0.00	0.0	0.0	0.0
	3	0.00	0.00	0.00	0.1	0.0	0.1
	4	0.05	−0.04	0.00	13.2	7.6	5.5
C:C	1	0.00	0.00	0.00	0.1	0.0	0.0
	2	0.00	0.00	0.00	0.0	0.0	0.0
	3	0.00	0.00	0.00	0.0	0.1	0.1
	4	0.01	0.17	0.17	6.9	0.1	6.8

[a]The electronic population analysis was achieved with the CHELPG formalism.

scavenger, quercetin is indeed an effective electron donor and is thus able to transfer some electron density to the positively charged 3-*O*-methylcyanidin. This efficient electron coupling decreases the positive charge of 3-*O*-methylcyanidin, thus stabilizing again the complex, decreasing Coulomb repulsion. Moreover, the ground-state CT allows stabilization of low-lying unoccupied orbitals of 3-*O*-methylcyanidin, a precursor effect of the vis absorption shift typical of copigmentation. Only slight or even nonsignificant CTs are expected in the dimer ground states (Table 2, **Q:Q** and **C:C**). However, for the **Q:Q** dimers, the parallel orientation (orientation **4**) presents a significant CT (q_{GS}^{CT} around 0.04 e, see Table 2, **C:Q**). In this specific case corresponding to the so-called parallel displaced stacking, the arrangement of dipole moments on each monomer favors CT (Scheme 2). On the contrary, for the antiparallel orientations

Scheme 2. (a) Parallel and (b) Antiparallel Dipole Displaced Stacking, Allowing and Not Allowing CT, Respectively, in Q:Q Complexes

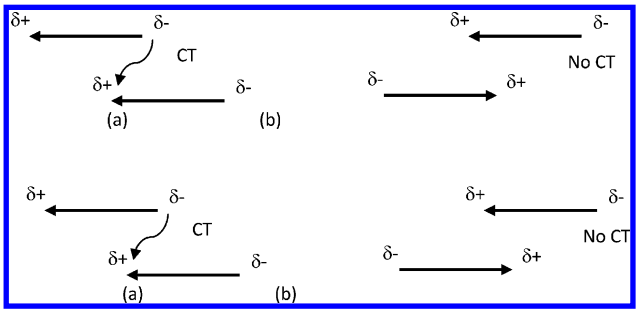

(orientations **1**−**3**), CT is unfavorable (Scheme 2b). CT is definitely unlikely for the **C:C** dimers as both monomers are positively charged, thus dramatically decreasing their electron-donating capacity.

4.2. UV−vis Properties. In the copigmentation complex studied here, both the highest occupied molecular orbital (H or HOMO) and H − 1 correspond to H of quercetin and 3-*O*-methylcyanidin, respectively, while the lowest unoccupied molecular orbital (L or LUMO) and L + 1 correspond to L of 3-*O*-methylcyanidin and quercetin, respectively (Figure 4). According to the linear combination of atomic orbital (LCAO) analysis, H is equally on the A- and C-rings and half on the B-ring of the quercetin moiety, while L is mainly located on the A- and C-rings of the 3-*O*-methylcyanidin moiety (∼77%, see Supporting Information, Table S11).

As a direct consequence of this redistribution in the frontier orbitals, the H → L gap (E_{gap}) of the complex (e.g., 5.8 eV in orientation **5** of **C:Q**) is dramatically and slightly reduced compared to quercetin (E_{gap} = 7.1 eV) and 3-*O*-methylcyanidin (E_{gap} = 6.1 eV), respectively (Figure 4).

For orientations **4** and **5** of **C:Q**, the maximum absorption wavelength is mainly assigned to the H → L electronic transition, corresponding to a CT excited state. As for the ground state, CT occurs from quercetin to 3-*O*-methylcyanidin.[69] This CT absorption band corresponds to the observed bathochromic shift typical of copigmentation. We must insist that it is not strictly a vis absorption band shift but actually a new band that appears, corresponding to the CT excited state that can only occur in π-stacking complexes. The oscillator strength of this new band can be relatively high (f being up to 0.41, see Table 3). Nonetheless this strongly depends on the orientation. On the one hand, when CT is important (see Table 2, for e.g., orientation **5** for which q^{CT} is 0.73), the CT excited-state contribution is high, and the bathochromic reaches −0.23 eV (37.8 nm). This is attributed to an efficient overlap between H and L, involving A- and C- and B-rings of both partners. The importance of CT is also correlated to the change in the dipole moment from the ground to the excited states (Table 2). On the other hand, when the H − 1 → L transition (i.e., involving only the 3-*O*-methylcyanidin fragment)

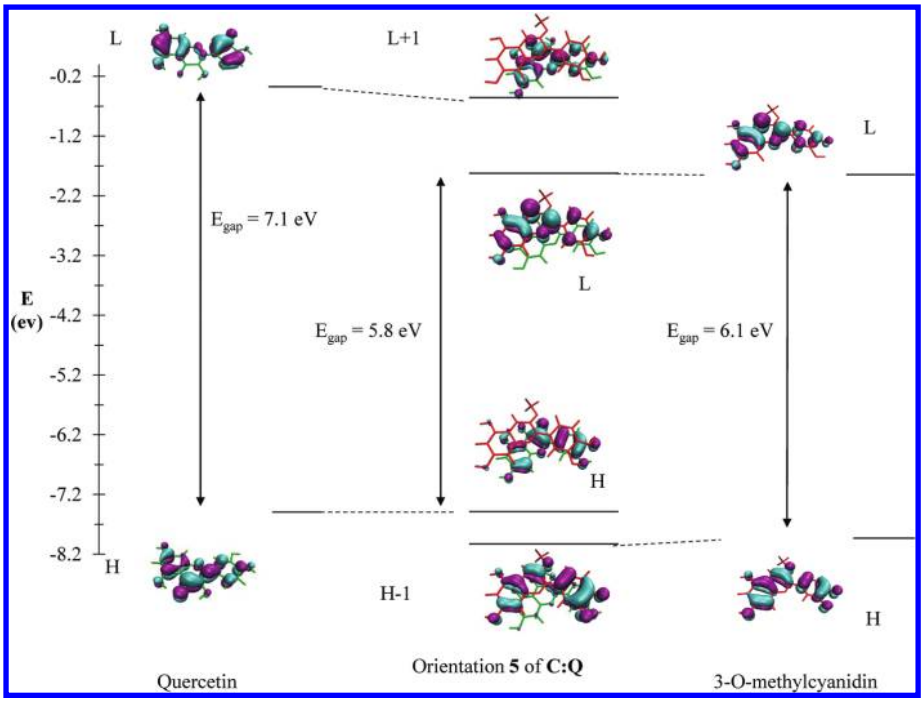

Figure 4. MO correlation diagram of quercetin, orientation **5** of **C:Q** and 3-*O*-methylcyanidin.

Table 3. Maximum Vertical Excitation Energies (E_{max}, eV), Absorption Wavelengths (λ_{max}, nm), Oscillator Strengths (f), MO Descriptions (%), Excitation Energy Shifts (ΔE_{max}, eV), Absorption Wavelength Shifts ($\Delta\lambda_{max}$, nm), and Boltzmann Weighted Bathochromic Shift ($\Delta\lambda_{bolt}$, nm) of C:Q, Q:Q, and C:C at the TD-ωB97X-D/cc-pVDZ Level of Theory Using SS-PCM Implicit Solvent Model[a]

complex	orientation	E_{max}	λ_{max}	f	MO description	ΔE_{max}	$\Delta\lambda_{max}$	$\Delta\lambda_{bolt}$
	1	2.81	441.7	0.41	H − 1 → L (65.0)	−0.02	3.7	
	2	2.79	443.7	0.33	H − 1 → L (66.3)	−0.04	5.7	
C:Q	**3**	2.76	448.7	0.27	H − 1 → L (66.3)	−0.07	10.8	22.9
	4	2.70	458.9	0.33	H → L (56.8)	−0.13	20.9	
	5	2.61	475.8	0.05	H → L (66.1)	−0.23	37.8	
	1	3.73	332.8	0.82	H − 1 → L (59.5)	0.01	−1.1	
	2	3.73	332.5	0.95	H → L (52.7)	0.02	−1.5	
Q:Q	**3**	3.74	331.7	0.89	H − 1 → L (40.5) H → L + 1 (53.5)	0.03	−2.3	−4.1
	4	3.78	328.3	0.86	H − 1 → L (37.6)	0.06	−5.7	
	1	2.89	429.1	0.72	H → L (59.5)	0.06	−8.8	
	2	2.88	430.9	1.07	H − 1 → L (54.7)	0.05	−7.1	
C:C	**3**	2.88	430.3	0.79	H − 1 → L (56.7)	0.05	−7.7	−8.3
	4	2.90	427.9	0.53	H − 1 → L (49.6) H → L (34.7)	0.07	−10.0	

[a]The energy and wavelength shifts are calculated with respect to the corresponding free flavonoid for **Q:Q** and **C:C** and with respect to 3-*O*-methylcyanidin for **C:Q**.

contributes to the maximum absorption band, the oscillator strength is increased, while the CT contribution decreases (Table 3). For example, for orientation **1**, both B-rings do not interact, decreasing H and L overlap between both partners, making the H → L electronic transition improbable. The CT excited-state contribution is weak, and the maximum absorption energy (E_{max}) is similar to that of 3-*O*-methylcyanidin, preventing bathochromic shift (ΔE_{max} = −0.02 eV, see Table 3).

The bathochromic shift experimentally observed thus appears as a global effect that must be attributed to the different orientations of the copigmentation complexes. The Boltzmann weighted bathochromic shift ($16.2\%\cdot\lambda_{max}^{orientation1} + 12.9\%\cdot\lambda_{max}^{orientation2} + 7.0\%\cdot\lambda_{max}^{orientation3} + 19.9\%\cdot\lambda_{max}^{orientation4} + 44.0\%\cdot\lambda_{max}^{orientation5}$) is 0.14 eV (23 nm) (Table 3). This correctly fits with the experimental bathochromic shift obtained with the cyanidin/quercetin couple, i.e., 11.7 nm.[20] The theoretical evaluation slightly overestimated this shift,[70] however it has been discussed that under these experimental conditions, the complete complexation cannot be reached, which may slightly induce underestimation of $\Delta\lambda_{max}$.[30] This confirms again the robustness of the methodology described above. The noncovalent dimers exhibit slight hypsochromic shifts with respect to the monomers (quercetin and 3-*O*-methylcyanidin), i.e., lower than 0.06 eV (−5.7 nm) and up to 0.07 eV (−10 nm) for **Q:Q** and for **C:C**, respectively (Table 3). The maximum wavelengths are not assigned to H → L only, as in the monomers (Table 3), but to a mixture of H − 1→ L, H → L, and H → L + 1 transitions. This partially explains the hypsochromic shifts. Due to symmetry between both monomers, mainly in the parallel orientations, H and H − 1 on one hand and L and L + 1 on the other hand are very close in energy; confirming that the shift is slight. Such hypsochromic shifts have been observed in self-association of anthocyanins. However it may only slightly affect the global UV−vis spectra of pigment/copigment mixtures because of the small occurrence of dimers and the low shift values when averaged over all possible orientations.

5. CONCLUSION

The present work has adopted, after a careful benchmarking, a theoretical methodology to reliably evaluate the formation of π-stacking complexes, as demonstrated for the copigmentation of anthocyanins by flavonols. The evaluation of π-stacking complexes is achieved by the BSSE-corrected B3P86 DFT functional including the Grimme's dispersive term (with the s_6 parameter adjusted to a value of 0.780). The robustness of this method was cross-checked according to high-level SCS-MP2 calculations for the evaluation of the binding energies. By using the former and less-costly method, different possible π-stacking complexes of flavonoids can be predicted in solution or in plant cells. The driving force in the formation of cyanidin:flavonol complexes appears to be $\pi-\pi$ interactions, H-bonding only slightly contributing to the stabilizing energies. This observation agrees with experimental data. The careful evaluation of the potential energy surface highlighted several possible orientations with significant Boltzmann weight. The weighted complexation energies also fit well with experimental values.

It must be stressed that in most in vitro studies in which UV−vis absorption properties are evaluated, the 1:1 binding definitely obtained.[71] Therefore in the present study only two-partner association (self-association and copigmentation complexes) has been considered. The formation of complexes of higher stoichiometry (tri-, tetra-, or pentamers) cannot be excluded in plant cell vacuoles where the pigment and copigment concentrations maybe quite high. Moreover in this case, pigments and copigments can be more complex,[72] providing large-scale molecular architectures, for which the optical properties cannot be achieved at the quantum level. Moreover, under strongly acidic solutions (typically used to measure bathochromic shift typical of copigmentation), the presence of colored quinonoid bases ($pK_h \sim 4$) is neglected, also because neutral quinonoid bases typically bind flavonols less strongly than the corresponding flavylium ion (e.g., a factor of ∼3 for malvidin 3,5-di-*O*-glucoside and quercetin 3-*O*-rutinoside).[73]

The bathochromic shift typical of copigmentation, a major mechanism of color variation in plants, has been also accurately

evaluated using the ωB97X-D range-separated hybrid functional. In particular, the expected bathochromic shift experimentally observed with the cyanidin:quercetin pair is perfectly reproduced by theoretical calculations. It actually corresponds to the appearance of a new vis absorption band corresponding to a CT excited state. Again, taking all possible geometries into account together with their corresponding Boltzmann weights appeared mandatory to accurately reproduce the UV−vis absorption spectra. Quantum chemical calculations have thus allowed providing a detailed molecular orbital picture and thus a complete spectroscopic understanding of anthocyanin:flavonol copigmentation. We are confident that this methodology can be successfully applied in the near future to firmly rationalize the mechanism causing color variation in polyphenols, which occurs in plant and food. Indeed, controlling natural colors in the food industry and in modern "haute cuisine", such as molecular gastronomy, is a crucial point in the appreciation of quality by consumers.

■ ASSOCIATED CONTENT

Ⓢ Supporting Information

Standard MAD through the S22 set vs the s_6 parameter; potential energy surface for the antiparallel orientation of **C:Q** at optimized distance (z); energy diagrams of frontier orbitals of **C:Q**, **Q:Q**, and **C:C** as obtained with B3P86 and ωB97X-D; 3D distributions of the frontier orbitals for quercetin, 3-*O*-methylcyanidin, **C:Q**, **Q:Q**, and **C:C**; theoretical UV−vis spectra for the five orientations of **C:Q**; comparison of λ_{max} at the TD-B3P86 and TD-ωB97X-D level of theory; BSSE-corrected and uncorrected interaction energies of **C:Q**, **Q:Q**, and **C:C** in the gas phase; calculated UV−vis properties using IEFPCM; BSSE-corrected and uncorrected interaction energies of [cyanidin:quercetin] complex; and MO-LCAO coefficients for the five orientations of **C:Q**. This material is available free of charge via the Internet at http://pubs.acs.org.

■ AUTHOR INFORMATION

Corresponding Author

*E-mail: patrick.trouillas@unilim.fr. Tel.: +33 (0) 555 435 927.

Notes

The authors declare no competing financial interest.

■ ACKNOWLEDGMENTS

The authors thank the "Conseil Régional du Limousin" for financial support and CALI (CAlcul en LImousin) for computing facilities. Research in Limoges is also supported by COST actions (FA1003 "East-West Collaboration for Grapevine Diversity Exploration and Mobilization of Adaptive Traits for Breeding" and 0804 "Chemical Biology with Natural Compounds"). Financial support by the MICINN of Spain (project CTQ2011-27253) is gratefully acknowledged.

■ REFERENCES

(1) Hertog, M. G.; Feskens, E. J.; Hollman, P. C.; Katan, M. B.; Kromhout, D. *Lancet* **1993**, *342*, 1007−1011.
(2) Commenges, D.; Scotet, V.; Renaud, S.; Jacqmin-Gadda, H.; Barberger-Gateau, P.; Dartigues, J. F. *Eur. J. Epidemiol.* **2000**, *16*, 357−363.
(3) Saller, R.; Meier, R.; Brignoli, R. *Drugs* **2001**, *61*, 2035−2063.
(4) Gazak, R.; Marhol, P.; Purchartova, K.; Monti, D.; Biedermann, D.; Riva, S.; Cvak, L.; Kren, V. *Process Biochem.* **2010**, *45*, 1657−1663.
(5) *Flavonoids in Health and Disease*; Rice-Evans, C. A., Packer, L., Eds.; Dekker: New York, 1998; pp 281−316.
(6) Ballester, A.-R.; Molthoff, J.; de Vos, R.; te Lintel Hekkert, B.; Orzaez, D.; Fernández-Moreno, J.-P.; Tripodi, P.; Grandillo, S.; Martin, C.; Heldens, J.; Ykema, M.; Granell, A.; Bovy, A. *Plant Physiol.* **2010**, *152*, 71−84.
(7) Yoshida, K.; Mori, M.; Kondo, T. *Nat. Prod. Rep.* **2009**, *26*, 884−915.
(8) Anouar, E. H.; Gierschner, J.; Duroux, J.-L.; Trouillas, P. *Food Chem.* **2012**, *131*, 79−89.
(9) Quartarolo, A. D.; Russo, N. *J. Chem. Theory Comput.* **2011**, *7*, 1073−1081.
(10) Harborne, J. B.; Mabry, T. J.; Mabry, H. *The Flavonoids*; Chapman and Hall: London, 1975; pp 214−266.
(11) Markakis, P.; Ed., *Anthocyanins as Food Colors*: Academic Press: Waltham, MA, 1982; pp 1−38.
(12) Timberlake, C. F.; Bridle, P. *J. Sci. Food Agric.* **1967**, *18*, 473−478.
(13) Brouillard, R.; Dangles, O. *Food Chem.* **1994**, *51*, 365−371.
(14) Bayer, E.; Egeter, H.; Fink, A.; Nether, K.; Wegmann, K. *Angew. Chem., Int. Ed.* **1966**, *5*, 791−798.
(15) Raymond, B. *Phytochem.* **1983**, *22*, 1311−1323.
(16) Boulton, R. *Am. J. Enol. Vitic.* **2001**, *52*, 67−87.
(17) Rustioni, L.; Bedgood, D. R., Jr; Failla, O.; Prenzler, P. D.; Robards, K. *Food Chem.* **2012**, *132*, 2194−2201.
(18) Stephen, J, B. *Phytochem.* **1999**, *50*, 1395−1399.
(19) Brouillard, R., *Anthocyanins as Food Colors*; Academic Press: Waltham, MA, 1982
(20) Dimitric, M. J. M.; Baranac, J. M.; Brdaric, T. P. *Spectrochim. Acta A* **2005**, *62A*, 673−680.
(21) Hunter, C. A.; Sanders, J. K. M. *J. Am. Chem. Soc.* **1990**, *112*, 5525−5534.
(22) Velu, S. S.; Buniyamin, I.; Ching, L. K.; Feroz, F.; Noorbatcha, I.; Gee, L. C.; Awang, K.; Wahab, I. A.; Weber, J.-F. F. *Chem.—Eur. J.* **2008**, *14*, 11376−11384.
(23) Rezazgui, O.; Boëns, B.; Teste, K.; Vergnaud, J.; Trouillas, P.; Zerrouki, R. *Tetrahedron Lett.* **2011**, *52*, 6796−6799.
(24) Aragó, J.; Sancho-García, J. C.; Ortí, E.; Beljonne, D. *J. Chem. Theory Comput.* **2011**, *7*, 2068−2077.
(25) Gierschner, J.; Cornil, J.; Egelhaaf, H.-J. *Adv. Mater.* **2007**, *19*, 173−191.
(26) Zondlo, N. J. *Nat. Chem. Biol.* **2010**, *6*, 567−568.
(27) Malien-Aubert, C.; Dangles, O.; Amiot, M. J. *J. Agric. Food Chem.* **2000**, *49*, 170−176.
(28) Alluis, B.; Perol, N.; El, h. H.; Dangles, O. *Helv. Chim. Acta* **2000**, *83*, 428−443.
(29) Ferreira, d. S. P.; Lima, J. C.; Freitas, A. A.; Shimizu, K.; Macanita, A. L.; Quina, F. H. *J. Phys. Chem. A* **2005**, *109*, 7329−7338.
(30) Alluis, B.; Dangles, O. *Helv. Chim. Acta* **2001**, *84*, 1133−1156.
(31) Baranac, J. M.; Petranovic, N. A.; Dimitric-Markovic, J. M. *J. Agric. Food Chem.* **1996**, *44*, 1333−1336.
(32) Brouillard, R.; Dangles, O. *Flavonoids* **1994**, 565−588.
(33) Riley, K. E.; Pitoňák, M.; Jurečka, P.; Hobza, P. *Chem. Rev.* **2010**, *110*, 5023−5063.
(34) Trouillas, P.; Fagnere, C.; Lazzaroni, R.; Calliste, C.; Marfak, A.; Duroux, J.-L. *Food Chem.* **2004**, *88*, 571−582.
(35) Anouar, E.; Kosinova, P.; Kozlowski, D.; Mokrini, R.; Duroux, J. L.; Trouillas, P. *Phys. Chem. Chem. Phys.* **2009**, *11*, 7659−7668.
(36) Grimme, S. *WIREs* **2011**, *1*, 211−228.
(37) Janesko, B. G.; Henderson, T. M.; Scuseria, G. E. *Phys. Chem. Chem. Phys.* **2009**, *11*, 443−454.
(38) Vydrov, O. A.; Voorhis, T. V. *J. Chem. Phys.* **2010**, *133*, 244103.
(39) Zhao, Y.; Truhlar, D. *Theor. Chem. Acc.* **2008**, *120*, 215−241.
(40) Grimme, S. *J. Comput. Chem.* **2004**, *25*, 1463−1473.
(41) Grimme, S. *J. Comput. Chem.* **2006**, *27*, 1787−1799.
(42) Grimme, S.; Antony, J.; Ehrlich, S.; Krieg, H. *J. Chem. Phys.* **2010**, *132*, 154104−154119.
(43) Trouillas, P.; Marsal, P.; Siri, D.; Lazzaroni, R.; Duroux, J.-L. *Food Chem.* **2006**, *97*, 679−688.
(44) Yanai, T.; Tew, D. P.; Handy, N. C. *Chem. Phys. Lett.* **2004**, *393*, 51−57.

(45) Chai, J.-D.; Head-Gordon, M. *J. Chem. Phys.* **2008**, *128*, 084106.
(46) Jacquemin, D.; Perpète, E.; Ciofini, I.; Adamo, C. *Theor. Chem. Acc.* **2011**, *128*, 127−136.
(47) Chai, J.-D.; Head-Gordon, M. *Phys. Chem. Chem. Phys.* **2008**, *10*, 6615−6620.
(48) Neese, F. *WIREs* **2012**, *2*, 73−78.
(49) Frisch, M. J.; Trucks, G. W.; Schlegel, H. B.; Scuseria, G. E.; Robb, M. A.; Cheeseman, J. R.; Scalmani, G.; Barone, V.; Mennucci, B.; Petersson, G. A.; Nakatsuji, H.; Caricato, M.; Li, X.; Hratchian, H. P.; Izmaylov, A. F.; Bloino, J.; Zheng, G.; Sonnenberg, J. L.; Hada, M.; Ehara, M.; Toyota, K.; Fukuda, R.; Hasegawa, J.; Ishida, M.; Nakajima, T.; Honda, Y.; Kitao, O.; Nakai, H.; Vreven, T.; Montgomery, J. A.; Peralta, J. E.; Ogliaro, F.; Bearpark, M.; Heyd, J. J.; Brothers, E.; Kudin, K. N.; Staroverov, V. N.; Kobayashi, R.; Normand, J.; Raghavachari, K.; Rendell, A.; Burant, J. C.; Iyengar, S. S.; Tomasi, J.; Cossi, M.; Rega, N.; Millam, J. M.; Klene, M.; Knox, J. E.; Cross, J. B.; Bakken, V.; Adamo, C.; Jaramillo, J.; Gomperts, R.; Stratmann, R. E.; Yazyev, O.; Austin, A. J.; Cammi, R.; Pomelli, C.; Ochterski, J. W.; Martin, R. L.; Morokuma, K.; Zakrzewski, V. G.; Voth, G. A.; Salvador, P.; Dannenberg, J. J.; Dapprich, S.; Daniels, A. D.; Farkas; Foresman, J. B.; Ortiz, J. V.; Cioslowski, J.; Fox, D. J. *Guassian 09*; Gaussian, Inc.: Pittsburgh, PA, 2009.
(50) Neese, F.; Wennmohs, F.; Hansen, A.; Becker, U. *Chem. Phys.* **2009**, *356*, 98−109.
(51) Singh, U. C.; Kollman, P. A. *J. Comput. Chem.* **1984**, *5*, 129−145.
(52) Besler, B. H.; Merz, K. M., Jr.; Kollman, P. A. *J. Comput. Chem.* **1990**, *11*, 431−439.
(53) Breneman, C. M.; Wiberg, K. B. *J. Comput. Chem.* **1990**, *11*, 361−373.
(54) Chirlian, L. E.; Francl, M. M. *J. Comput. Chem.* **1987**, *8*, 894−905.
(55) Sinnecker, S.; Rajendran, A.; Klamt, A.; Diedenhofen, M.; Neese, F. *J. Phys. Chem. A* **2006**, *110*, 2235−2245.
(56) Cossi, M.; Scalmani, G.; Rega, N.; Barone, V. *J. Chem. Phys.* **2002**, *117*, 43−54.
(57) Tomasi, J.; Mennucci, B.; Cammi, R. *Chem. Rev.* **2005**, *105*, 2999−3093.
(58) Improta, R.; Barone, V.; Scalmani, G.; Frisch, M. J. *J. Chem. Phys.* **2006**, *125*, 054103.
(59) Jurecka, P.; Sponer, J.; Cerny, J.; Hobza, P. *Phys. Chem. Chem. Phys.* **2006**, *8*, 1985−1993.
(60) Gráfová, L.; Pitoňák, M.; Řezáč, J.; Hobza, P. *J. Chem. Theory Comput.* **2010**, *6*, 2365−2376.
(61) Grimme, S. *J. Chem. Phys.* **2003**, *118*, 9095−9102.
(62) Antony, J.; Grimme, S. *J. Phys. Chem. A* **2007**, *111*, 4862−4868.
(63) Due to the size of the basis set (cc-pVDZ), the energy difference between the optimized B3P86-D2 and SCS-MP2 is (mainly) attributed to BSSE. For this comparison, interaction energies were not counterpoise corrected here, considering that BSSE effects were later incorporated.
(64) The surface error (E^S) is obtained in a statistical manner by integrating energy differences between the DFT functional under evaluation and the SCS-MP2 value (taken here as reference), as a function of the intermolecular distance.
(65) Jacquemin, D.; Bahers, T. L.; Adamo, C.; Ciofini, I. *Phys. Chem. Chem. Phys.* **2012**, *14*, 5383−5388.
(66) Grimme, S. *Angew. Chem., Int. Ed.* **2008**, *47*, 3430−3434.
(67) It must be stressed that Dimitric et al. used the cyanidin aglycone, while we used 3-*O*-methylcyanidin as a slightly better model of natural anthocyanins (see Section 1). Nonetheless we have also performed the calculation with the cyanidin:quercetin complexes, and we have obtained very similar results, as shown in the Supporting Information.
(68) Grimme, S.; Djukic, J.-P. *Inorg. Chem.* **2011**, *50*, 2619−2628.
(69) The differences in CT energies between B3P86 and wB97X-D were evaluated for **C:Q** for which the B3P86-D geometry was used (see Supporting Information, Table S7). Both functionals provided the same wavelength for the main electronic transition, i.e., the H − 1 → L transition having the highest oscillator strength f (E_{max} = 2.76 and 2.44 eV with ωB97X-D and B3P86, respectively). Nonetheless, the CT excited state corresponding to the H → L vertical transition is dramatically underestimated with B3P86 ($f = 3.0 \times 10^{-3}$). The ωB97X-D functional appeared much more relevant to study UV−vis absorption of $\pi-\pi$ polyphenol complexes as it exhibited an oscillator strength (f = 0.28) higher and more accurate with respect to experimental data.
(70) PCM seemed to be in better agreement with ref 20 (see Supporting Informations, Table S9). However, as explained in text the corresponding shift maybe slightly underestimated, showing that the trend obtained with SS-PCM appears in better agreement with most of experimental observations, which appear very consistent with the improvement proposed by this method.
(71) Brouillard, R.; Mazza, G.; Saad, Z.; Albrecht-Gary, A. M.; Cheminat, A. *J. Am. Chem. Soc.* **1989**, *111*, 2604−2610.
(72) Gonzalez-Manzano, S.; Mateus, N.; Freitas, V.; Santos-Buelga, C. *Eur. Food Res. Technol.* **2008**, *227*, 83−92.
(73) Dangles, O.; Brouillard, R. *Can. J. Chem.* **1992**, *70*, 2174−2189.